A Value Piking Method for Mixed Boundary Conditions in Inverse Scattering Problems

Fan Yin, Chang Chen, and Weidong Chen
University of Science and Technology of China, China

2022 Photonics & Electromagnetics Research Symposium (PIERS) | 978-1-6654-6023-1/22/$31.00 ©2022 IEEE | DOI: 10.1109/PIERS55526.2022.9792757

Abstract— In the inverse scattering problem (ISP) with mixed boundary conditions, conduct and dielectric scatterers coexist in the same region, which challenges the present quantitative inverse scattering methods. Moreover, to ensure the incident waves penetrating the lossy or high contrast objects, lower wavelength is applied in most inverse scattering applications, which results in a severely ill-posed problem. In this paper, we devise a quantitative inversion scheme alternately updating the contrast of dielectric scatterers and the T-matrix of conduct scatterers, where a value piking regularization is imposed for inhomogeneous objects with piecewise homogeneity. The proposed alternate parameter updating method (APUM) avoids the reconstruction deterioration from both of the large imaginary parts of conduct contrasts and the limited expansion order of the T-matrix. Then, the APUM is further improved by imposed a priori information for piecewise constant parameters of the conduct scatterers and the dielectric scatterers. The results with synthetic data and single-frequency Fresnel experimental data verify the effectiveness of the proposed method.

1. INTRODUCTION

Inverse scattering imaging has a wide applications, such as nondestructive testing [1, 2], biomedical imaging [3], geological exploration [4], through wall imaging [5], and ground penetrating radar [6]. Most of these applications are mixed boundary ISPs, of which dielectric and conduct objects exist in the same domain of interest (DOI). In the mixed boundary ISPs, incident wave is required to penetrate observed objects, while the skin effects of these lossy objects limit the wavelength. Imaging wavelength scale objects with mixed boundary conditions is a severely ill-posed problem [7].

Most quantitative methods such as the contrast source inversion (CSI) method [8, 9] can retrieve the complex permittivity. The CSI method solves the problem under electric field integral equation (EFIE) model and approximates the conduct scatterers by lossy dielectric scatterers according to the volume equivalence principle. The objects with zero imaginary parts in permittivity are dielectrics, while the ones with large imaginary parts are conductors. However, conduct scatterers in low frequency radio wave can approximate perfect electric conductors (PEC). The CSI method may fail in the case with high-loss dielectric scatterers or PEC scatterers where the large imagery components will corrupt the reconstructed results. To overcome these defects, the inverse T-matrix method is proposed to distinguish between conduct scatterers and dielectric scatterers [10]. The T-matrix coefficients of the scatterers are recovered by modeling the scattering of different types of scatterers [11]. Different from the EFIE model, the T-matrix model describes scattering by multipole expansion. The permittivity of the dielectric scatterer is obtained from the small term asymptotic approximations of T-matrix, which provides limited qualitative reconstruction [12]. Because the computational cost limits the expansion degrees, the approximations in the inverse T-matrix method are inaccurate. The reconstructions of dielectric scatterers in the inverse T-matrix method cannot achieve the same resolution as the CSI method. Therefore, a combined method to make advantage of both method is a possible way to improve the imaging quality.

Compared with the ISP for dielectric objects, the mixed boundary ISP applies lower frequency waves to penetrate the objects and requires higher imaging resolution, which results in a more severely ill-posed problem. Various types of regularization techniques directly impose constrains on solutions [13, 14]. Some of these constraints are not universal for practical problems. Most of objects in the applications of the ISP are neither edge smoothing nor sparse, which challenges the existing regularization methods. Recent researches focus on the inhomogeneous objects composed of compact piecewise homogeneous materials, such as the value piking (VP) method [15], the weakly convex discontinuity adaptive regularization [16], the Huber regularization method [17] and the hierarchical Bayesian method [18]. The methods [15–17] solve the nonlinear ISP with Gauss-Newton method, of which the convergence is not stable. The hierarchical Bayesian method solves the ISP with linear approximation, which unable to handle strong scatterers. All of these methods are based on the EFIE model, which are not suitable for the mixed condition ISP.

In this paper, we treated the mixed boundary ISP as an alternate inversion of the contrast of dielectrics and the T-matrix of conductors. The alternate parameter updating method (APUM) avoids the contrast interfered by the large imaginary parts of the conductors and improves the accuracy of the reconstructed T-matrix. Furthermore, we impose the value piking regularization for piecewise homogeneity objects in APUM. As the parameters are constant inside the PEC scatterers and the free space, the VP values for the PEC scatterers and the free space is fixed at the beginning of the iteration, which provides convenience for the calculation. The proposed method is verified on synthetic data and experimental data with mixed boundary objects.

2. FORMULATION OF THE PROBLEM

A typical 2D inverse scattering problem is presented in Fig. 1, where transverse magnetic (TM) case is considered with the longitude direction along the z-axis. Region D is the domain of interest (DOI) where the dielectric scatterers and the PEC scatterers are located. M receivers are located uniformly on the curve C at r_m with $m = 1, \ldots, M$. The objects in DOI are illuminated by I line sources at the curve C for P times.

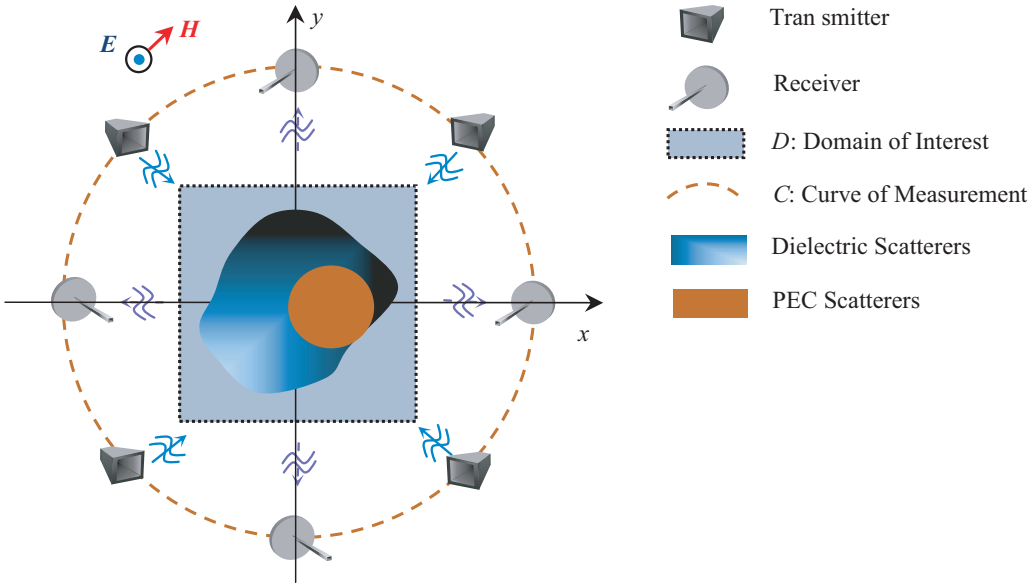

Figure 1: The geometry for the inverse-scattering problem: the dielectric scatterers and the PEC scatterers coexist in the domain of interest.

The DOI is discretized into N subunits in the forward problem, the volume equivalence model in the CSI is composed of the data equation and the state equation as

$$\begin{cases} \mathbf{e}_q^{sca} = \mathbf{G}_C \cdot \mathbf{w}_q \\ \mathbf{w}_q = \chi \odot \left(\mathbf{e}_q^{inc} + \mathbf{G}_D \cdot \mathbf{w}_q\right) \end{cases} \tag{1}$$

where subscript q represents the q-th illumination, and $\mathbf{e}_q^{sca}$, $\mathbf{e}_q^{inc}$, $\mathbf{w}_q$, χ, $\mathbf{G}_C$ and $\mathbf{G}_D$ are the measured scattering field, the incident field, the contrast source, the contrast, the Green operator at curve C and the Green operator at DOI respectively.

In the T-matrix model, the fields are represented as the form of multipole expansion with different expansion coefficients. As in [1], the equation of inverse T-matrix method is composed of the data equation and the state equation in matrix form as

$$\begin{cases} \mathbf{e}_q^{sca} = \mathbf{G} \cdot \mathbf{c}_q \\ \mathbf{c}_q = \mathbf{T}\left(\mathbf{i}_q + \mathbf{S} \cdot \mathbf{c}_q\right) \end{cases} \tag{2}$$

where $\mathbf{c}_q$ is the vector of the scattering coefficient, $\mathbf{i}_q$ is the vector of the incident field coefficient, $\mathbf{S}$ is the translational matrix and $\mathbf{T}$ is the transmitting matrix, known as the T-matrix. Assuming the expansion order $P = 0$, the scattering coefficients is proportional to the contrast sources

$$\mathbf{c}_q = j\frac{k_0^2 \pi R^2}{4}\mathbf{w}_q \tag{3}$$

Therefore, the T-matrix model and the volume equivalence model share the same data equation as

$$\begin{cases} \mathbf{e}_q^{sca} = \mathbf{G}_c \cdot \mathbf{w}_q \\ \mathbf{w}_q = \chi \odot \left(\mathbf{e}_q^{inc} + \mathbf{G}_D \cdot \mathbf{w}_q\right) \\ \mathbf{w}_q = \mathbf{T}\left(-j\frac{\eta_0}{4\pi R^2}\mathbf{i}_q + \mathbf{S} \cdot \mathbf{w}_q\right) \end{cases} \tag{4}$$

According to (4), both of the T-matrix and the contrast are updated from same contrast source. However, reconstructing the PEC scatterers and dielectric scatterers simultaneously also leads to the error accumulation on the contrast source. To avoid this error accumulation, the reconstructions of the T-matrix and the contrast are divided into the reconstruction of the T-matrix of PEC scatterers and the contrast of the dielectric scatterers. The contrast source is also divided into the contrast source of the dielectric scatterers and the one of PEC scatterers. Therefore, the ISP of the dielectric scatterers and the PEC scatterers are reformulated as

$$\begin{cases} \mathbf{e}_q^{\mathrm{die}} = \mathbf{G}_C^{\mathrm{pec}}\mathbf{w}_q^{\mathrm{die}} \\ \mathbf{w}_q^{\mathrm{die}} = \chi^{\mathrm{die}} \odot \left(\mathbf{e}_{q0}^{\mathrm{pec}} + \mathbf{G}_D^{\mathrm{pec}}\mathbf{w}_q^{\mathrm{die}}\right) \end{cases} \tag{5}$$

and

$$\begin{cases} \mathbf{e}_q^{pec} = \mathbf{G}_C^{\mathrm{die}}\mathbf{w}_q^{\mathrm{pec}} \\ \mathbf{w}_q^{\mathrm{pec}} = \mathbf{T}^{\mathrm{pec}}\left(-j\frac{\eta_0}{4\pi R^2}\mathbf{i}_{q0}^{\mathrm{die}} + \mathbf{S}^{\mathrm{die}} \cdot \mathbf{w}_q^{\mathrm{pec}}\right) \end{cases} \tag{6}$$

where $\mathbf{e}_q^{pec} + \mathbf{e}_q^{die} = \mathbf{e}_q^{die} + \mathbf{e}_q^{pec} = \mathbf{e}_q$ and $\mathbf{i}_q^{die}$ is the multipole coefficients of $\mathbf{e}_q^{die}$. $\mathbf{e}_q^{pec}$ is the total field of an equivalence problem where the dielectric scatterers are treated as the free space. $\mathbf{e}_q^{die}$ is the total field of an equivalence problem where the PEC scatterers are treated as the free space. $\mathbf{G}_C^{pec}$ and $\mathbf{G}_D^{pec}$ are the Green operators with PEC scatterers as the background. $\mathbf{G}_C^{die}$ is the Green operator with dielectric scatterers as the background. $\mathbf{S}^{die}$ is the translational matrix with dielectric scatterers as the background. The dielectric scatterers and the PEC scatterers are updated alternately by solving (5) and (6).

3. THE VP REGULARIZATION

As the mixed boundary ISP is ill-posed, VP regularization is imposed for the piecewise constant parameters to constrain the solution space.

Given the initial guess of the PEC scatterers, solving (5) is carried out by the minimization of the cost function as

$$f\left(\mathbf{w}_q^{die}, \chi^{die}, \mathbf{c}\right) = \frac{\sum_q \|\gamma_q\|_2^2}{\sum_q \left\|\chi^{\mathrm{die}} \odot \mathbf{e}_{q0}^{\mathrm{pec}}\right\|_2^2} + \frac{\sum_q \left\|\mathbf{r}_q^{\mathrm{die}}\right\|_2^2}{\sum_q \left\|\mathbf{e}_q^{\mathrm{die}}\right\|_2^2} + \gamma\frac{\sum_q \kappa_q\left(\mathbf{w}_q^{die}, \mathbf{c}_\chi\right)}{\sum_q \left\|\chi^{\mathrm{die}} \odot \mathbf{e}_{q0}^{\mathrm{pec}}\right\|_2^2} \tag{7}$$

where γ_q and $\mathbf{r}_q^{die}$ are the state error and the data error defined as

$$\begin{aligned} \gamma_q &= \chi^{\mathrm{die}} \odot \left(\mathbf{e}_{q0}^{\mathrm{pec}} + \mathbf{G}_D^{\mathrm{pec}}\mathbf{w}_q^{\mathrm{die}}\right) - \mathbf{w}_q^{\mathrm{die}} \\ \mathbf{r}_q^{\mathrm{die}} &= \mathbf{e}_q^{sca} - \mathbf{G}_C^{\mathrm{pec}}\mathbf{w}_q^{\mathrm{die}} \end{aligned} \tag{8}$$

κ_q is the VP function of the q-th illumination with the form

$$\kappa_q\left(\mathbf{w}_q^{die}, \mathbf{c}_\chi\right) = \sum_{\upsilon=1}^{\Upsilon}\sum_{n=1}^{N} b_\upsilon^{\Upsilon}\left[\mathbf{w}_q^{die}(n), \mathbf{c}_\chi\right]\left|g\left[\mathbf{w}_q^{die}(n), \mathbf{c}_\chi(\upsilon)\right]\right|^2 \tag{9}$$

where $\mathbf{c}_\chi$ is the array of VP values for the contrast. Function $g(\bullet)$ is the VP error between the n-th elements and the υ-th VP value as

$$g\left[\mathbf{w}_q^{die}(n), \mathbf{c}_\chi(\upsilon)\right] = \delta_\upsilon^H\left[\mathbf{c}_\chi(\upsilon) \cdot \left(\mathbf{e}_{q0}^{\mathrm{pec}} + \mathbf{G}_D^{\mathrm{PEC}}\mathbf{w}_q^{die}\right) - \mathbf{w}_q^{die}\right] \tag{10}$$

where δ_υ is a unit vector with the υ-th elements nonzero only. Function $b_\upsilon(\bullet)$ is the weight function defined in [15]. With the initial values of χ^{die} and $\mathbf{c}_\chi$, the minimization of (7) is carried out by

Polak-Ribière-Polyak conjugate gradient method [19] and leads to $\mathbf{w}_q^{die}$. Given $\mathbf{w}_q^{die}$, χ^{die} is updated as the way in the CSI explicitly [8]. Updating $\mathbf{c}$ is carried out by the minimization of (7) as well, while $\mathbf{w}_q^{die}$ and χ^{die} remain constant.

Given the dielectric scatterers, the cost function for solving (6) is

$$f\left(\mathbf{w}_q^{\text{pec}}, \mathbf{T}^{\text{pec}}\right) = \frac{\sum_q \left\|\mathbf{r}_q^{\text{pec}}\right\|_2^2}{\sum_q \left\|\mathbf{e}_q^{\text{pec}}\right\|_2^2} + \frac{\sum_q \left\|\varsigma_q\right\|_2^2}{\sum_q \left\|-j\eta_0 \mathbf{T}^{\text{pec}} \mathbf{i}_{q0}^{\text{die}} / 4\pi R^2\right\|_2^2} + \gamma \frac{\sum_q \kappa_q\left(\mathbf{w}_q^{\text{pec}}, \mathbf{c}_T\right)}{\sum_q \left\|-j\eta_0 \mathbf{T}^{\text{pec}} \mathbf{i}_{q0}^{\text{die}} / 4\pi R^2\right\|_2^2} \tag{11}$$

where ς_q and $\mathbf{r}_q^{pec}$ are the state error and the data error defined as

$$\begin{aligned} \varsigma_q &= \mathbf{T}^{\text{pec}}\left(-j\frac{\eta_0}{4\pi R^2}\mathbf{i}_{q0}^{\text{die}} + \mathbf{S}^{\text{die}}\mathbf{w}_q^{\text{pec}}\right) - \mathbf{w}_q^{\text{pec}} \\ \mathbf{r}_q^{\text{pec}} &= \mathbf{e}_q^{sca} - \mathbf{G}_C^{\text{die}}\mathbf{w}_q^{\text{pec}} \end{aligned} \tag{12}$$

κ_q is the VP function of the q-th illumination with the form

$$\kappa_q\left(\mathbf{w}_q^{\text{pec}}, \mathbf{c}_T\right) = \sum_{\upsilon=1}^{2}\sum_{n=1}^{N} b_\upsilon^2 \left[\mathbf{w}_q^{\text{pec}}(n), \mathbf{c}_T\right] \left|g\left[\mathbf{w}_q^{\text{pec}}(n), \mathbf{c}_T(\upsilon)\right]\right|^2 \tag{13}$$

The VP value $\mathbf{c}_T$ in (11) is constant, for the element of PEC T-matrix remain constant as

$$t_n^0 \approx -\left[\frac{\pi}{2\ln\left(2/\gamma k_0 R\right)}\right]^2 + j\frac{\pi}{2\ln\left(2/\gamma k_0 R\right)} \tag{14}$$

where R is the radius of the discrete elements. Excepting the updating of VP value, the minimization of (11) is carried out with *Polak-Ribière-Polyak* conjugate gradient method as well as (7). Thus, the contrast of the dielectric scatterers and the T-matrix of the PEC scatterers are updated alternately, which improves the quantitative reconstruction of the mixed boundary ISP.

The regularization parameter γ in (7) and (11) determines the convergency of iteration. Both of the VP regularization and the state equation constrain the solution space of the data equation. However, the solution space determined by the VP regularization may be different with the one determined by the state equation. An illustrative map of searching the solution space with and without the VP regularization is depicted in Fig. 2.

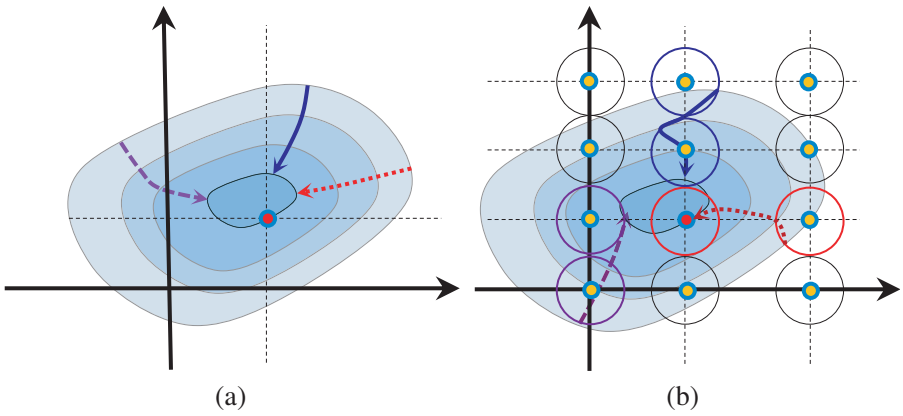

Figure 2: Illustrative map of (a) searching the solution space without the VP regularization, and (b) searching with the VP regularization.

The closed curves in Fig. 2 represents the contours of the cost function without the VP regularization. The closer to the inner contour, the smaller the cost function is. The red dot on the innermost contour is the truth-value. The purple dash line, the blue line and the red dot line are three searching routes with different initial values. In Fig. 2(a), the searching routes are determined by the gradient of the cost function, which is perpendicular to the tangent of the contour. The yellow dots in Fig. 2(b) are the VP values around which the circle indicates the contours of the

VP regularization. In Fig. 2(b), both of the cost function and the nearest VP value determine the searching routs. However, in the case that the gradient of the cost function is opposite to the gradient of the VP regularization, the searching route cannot be guided to the truth-value. For example, the blue line and the purple dash line in Fig. 2(b) fall in the local optimal results, where the contour of the VP regularization is tangent to the contour of the cost function without the VP regularization.

To address this problem, the VP regularization is activated only when the VP term is smaller than the other term of the cost function, by which the red dot line in Fig. 2(b) leads to the truth-value. Therefore, the regularization parameter is set according to (15).

4. RESULTS AND DISCUSSIONS

In this section, we verified the proposed method against the synthetic data from method of the moments (MOM) and the experimental laboratory-controlled data. The forward problem is solved with the CG-FFT method to acquire the measurement data [20]. Ten percent additive white Gaussian noise (AWGN) is added to the synthetic data for all tests. The performances of the new inversion method is compared with the CSI and inverse T-matrix.

In the first example, we use the synthetic data to verified the proposed method. The object is consist of a square copper cylinder and a circular dielectric cylinder. The copper cylinder with

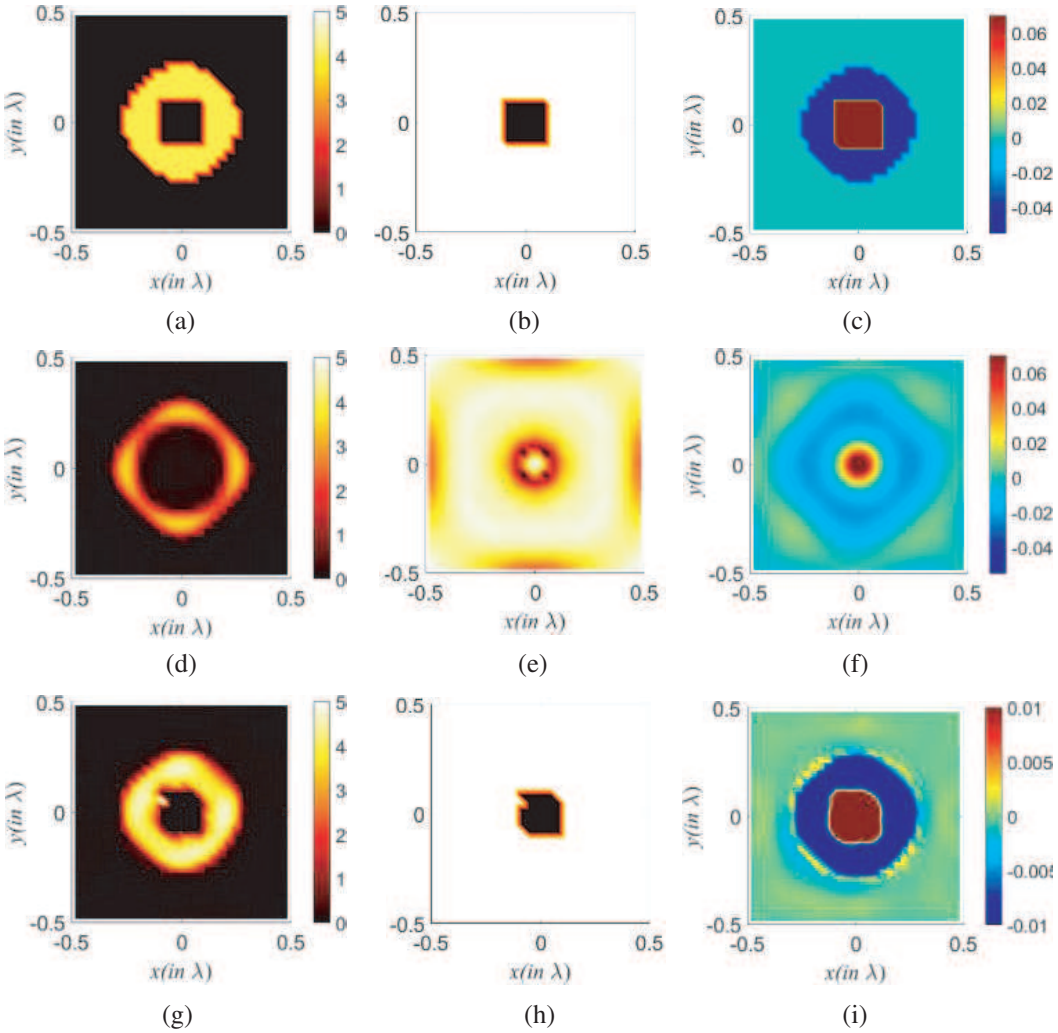

Figure 3: (a) Real parts of original contrasts, (b) image parts of original contrasts and (c) image parts of original T-matrix. (d) Real parts of reconstructed contrasts with normal CSI, (e) image parts of reconstructed contrasts with normal CSI and (f) image parts of reconstructed T-matrix with inverse T-matrix. (g) Real parts of reconstructed contrasts with proposed method, (h) image parts of reconstructed contrasts with APUM and (i) reconstructed conduct T-matrix with proposed method.

side length $\lambda_0/5$ is wrapped in the dielectric cylinder with radius $2\lambda_0/5$. The contrast of the dielectric scatterers is 4 and the conductivity of the copper is 6×10^7 S/m. The DOI is a square with sides of length λ_0, which is surrounded by the measurement curve C with radius $3\lambda_0$. Forty transmitters and forty receivers are equally spaced in the measurement curve. The discrete form of the problem is obtained by dividing the DOI into 30×30 subsquares. The forward problems are calculated with a finer 50×50 grid mesh to avoid inverse crime. The reconstructed results with normal CSI, inverse T-matrix and the proposed method are shown in Fig. 3. The dielectric cylinder and the copper cylinder are reconstructed by proposed method in Fig. 3(g) and Fig. 3(h) respectively. In contrast, the normal CSI failed to reconstruct both of the copper cylinder and the dielectric cylinder. Compared with the result of inverse T-matrix method in Fig. 3(f), the result of the proposed method in Fig. 3(j) retains the shape edges of the objects, which shows the effective of VP regularization.

In the second example, the proposed method is tested on the dataset "*FoamMetExt*" collected by Institute Fresnel [21], where a copper cylinder is placed against a foam cylinder in DOI. The radius of the copper cylinder and the foam cylinder are 28.5 mm and 80 mm respectively. The foam cylinder has $\varepsilon_r = 1.45 \pm 0.15$. Eighteen sources illuminate the DOI in turn around a circle while the scattering field of each illumination is measured at 241 receiving locations in the same circle. The radius of the measurement circle is 1.67 m. The data at 4 GHz is used for reconstruction. The DOI

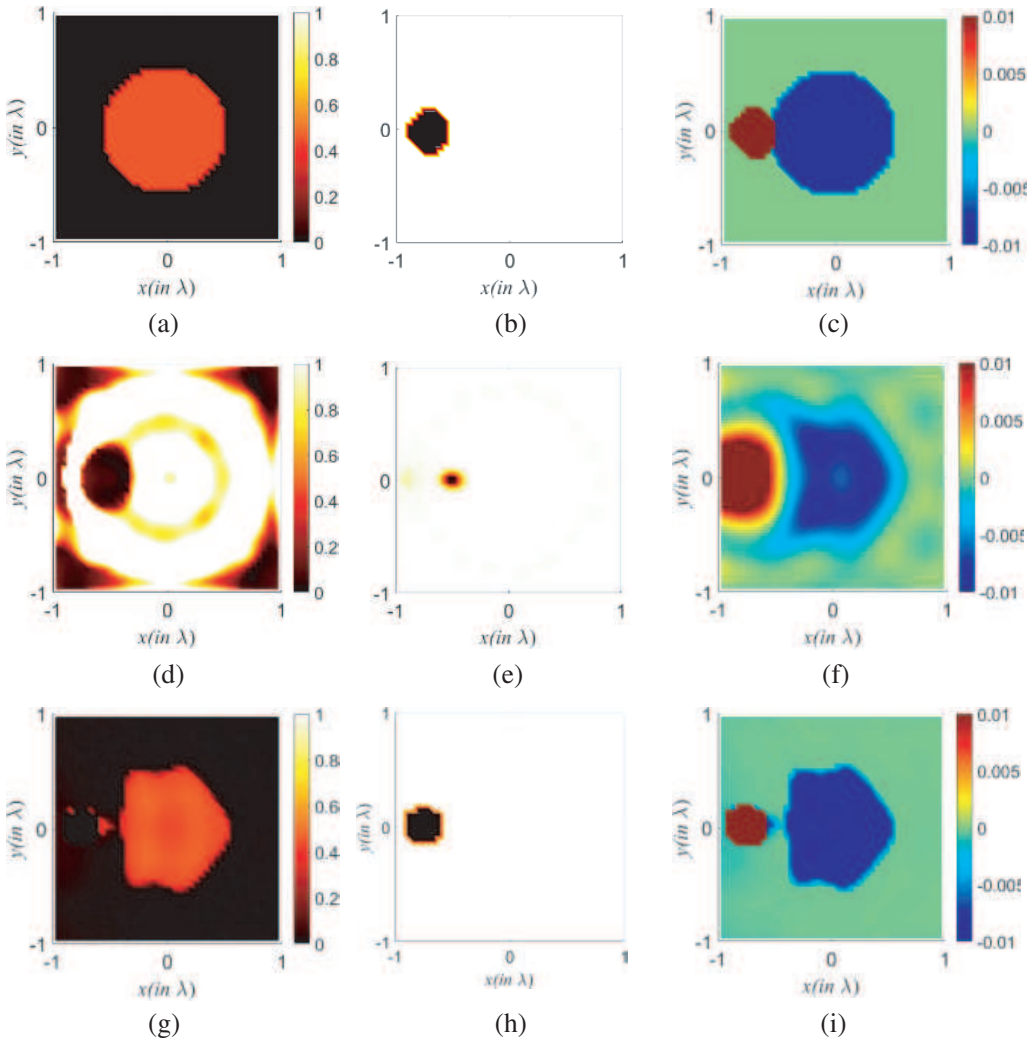

Figure 4: (a) Real parts of original contrasts, (b) image parts of original contrasts and (c) image parts of original T-matrix. (d) Real parts of reconstructed contrasts with normal CSI, (e) image parts of reconstructed contrasts with normal CSI and (f) image parts of reconstructed T-matrix with inverse T-matrix. (g) Real parts of reconstructed contrasts with APUM, (h) image parts of reconstructed contrasts with APUM and (i) reconstructed conduct T-matrix with APUM.

is of size 150 mm × 150 mm and discrete as 44 × 44 subsquares. Fig. 4 compares the reconstruction result of proposed method with the result of inverse T-matrix and the CSI, of which the result of proposed method is better than the other results.

The CSI failed to reconstruct the copper cylinder in Fig. 4(e), which compromises the reconstruction of the dielectric object in Fig. 4(d). In contrast, the foam cylinder reconstructed by the proposed method in Fig. 4(g) has clear edges. Compared with the result of the inverse T-matrix method in Fig. 4(i), the result of proposed method has sharper edges, which shows the effectiveness of the regularization.

5. CONCLUSION

In the ISP with mixed boundary condition, the contrast of the PEC scatterers has infinite large imaginary parts, which can disturb the reconstruction of the dielectric scatterers in the CSI. The inverse T-matrix can handle the PEC scatterers and the dielectric scatterers simultaneously. However, the quality of the reconstructed result in the inverse T-matrix method is limited by the order of the multipole expansion, which suffers from the ill-posedness of the mixed boundary ISP. In this paper, we provide a hybrid parameter model consist of the T-matrix and the contrast. The dielectric contrast and the PEC T-matrix are updated alternately, which avoids the interferences between the reconstruction of the dielectric scatterers and the PEC scatterers. The VP regularization is introduced into the cost function to constrain the solution space, of which the objects are composed of compact piecewise homogeneous materials. The minimization of the cost function is solved by Polak-Ribière-Polyak conjugate gradient method, which ensure the convergence. The proposed method is verified on the synthetic data and the experimental data. The results showed that the proposed method is superior to other algorithms when regular-shaped scatterers with different boundary conditions are at hand.

ACKNOWLEDGMENT

This work was supported in part by the National Natural Science Foundation of China under Grant 61971392.

REFERENCES

1. Hassen, F. B., Y. Boukari, and H. Haddar, "Application of the linear sampling method to identify cracks with impedance boundary conditions," *Inverse Probl. Sci. En.*, Vol. 21, No. 2, 210–234, Mar. 2013.
2. Benedetti, M., M. Donelli, A. Martini, M. Pastorino, A. Rosani, and A. Massa, "An innovative microwave-imaging technique for nondestructive evaluation: Applications to civil structures monitoring and biological bodies inspection," *IEEE Trans. Instrum. Meas.*, Vol. 55, No. 6, 1878–1884, Dec. 2006.
3. Neira, L. M., B. D. V. Veen, and S. C. Hagness, "High-resolution microwave breast imaging using a 3-D inverse scattering algorithm with a variable-strength spatial prior constraint," *IEEE Trans. Antennas Propag.*, Vol. 65, No. 11, 6002–6014, Nov. 2017.
4. Gürbüz, T. U., B. Aslanyürek, E. P. Karabulut, and I. Akduman, "An efficient nonlinear imaging approach for dielectric objects buried under a rough surface," *IEEE Trans. Geosci. Remote Sens.*, Vol. 52, No. 5, 3013–3022, May 2014.
5. Chu, Y., K. Xu, Y. Zhong, X. Ye, T. Zhou, X. Chen, and G. Wang, "Fast microwave through wall imaging method with inhomogeneous background based on Levenberg-Marquardt Algorithm," *IEEE Trans. Microw. Theory Techn.*, Vol. 67, No. 3, 1138–1147, Mar. 2019.
6. Donato, L. D. and L. Crocco, "Model-based quantitative cross-borehole GPR imaging via virtual experiments," *IEEE Trans. Geosci. Remote Sens.*, Vol. 53, No. 8, 4178–4185, Aug. 2015.
7. Chen, X., *Computational Methods for Electromagnetic Inverse Scattering*, Wiley, Hoboken, NJ, USA, 2018.
8. Crocco, L., M. D'Urso, and T. Isernia, "Testing the contrast source extended Born inversion method against real data: The TM case," *Inv. Prob.*, Vol. 21, 33–50, 2005.
9. Yu, C., L. P. Song, and Q. H. Liu, "Inversion of multi-frequency experimental data for imaging complex objects by a DTA-CSI method," *Inv. Prob.*, Vol. 21, 165–178, 2005.
10. Ye, X., X. Chen, Y. Zhong, and R. Song, "Simultaneous reconstruction of dielectric and perfectly conducting scatterers via T-matrix method," *IEEE Trans. Antennas Propag.*, Vol. 61, No. 7, 3774–3781, Jul. 2013.

11. Waterman, P. C., "Matrix formulation of electromagnetic scattering," *Proc. IEEE*, Vol. 53, 805–811, 1965.
12. Song, R., X. Ye, and X. Chen, "Reconstruction of scatterers with four different boundary conditions by T-matrix method," *Inverse Probl. Sci. En.*, Vol. 23, No. 4, 601–616, May 2014.
13. Oliveri, C., P. Rocca, and A. Massa, "A Bayesian compressive sampling based inversion for imaging sparse scatterers," *IEEE Trans. Geosci. Remote Sens.*, Vol. 49, No. 10, 3993–4006, Oct. 2011.
14. Sun, S., B. J. Kooij, and A. G. Yarovoy, "Linearized 3-D electromagnetic contrast source inversion and its applications to half-space configurations," *IEEE Trans. Geosci. Remote Sens.*, Vol. 55, No. 6, 3375–3487, Jun. 2017.
15. Bulcke, S. V. D., A. Franchois, and D. D. Zutter, "Piecewise smoothed value picking regularization applied to 2-D TM and TE inverse scattering," *IEEE Trans. Antennas Propag.*, Vol. 61, No. 6, 3261–3269, Jun. 2013.
16. Bai, F., A. Pižurica, B. Truyen, W. Philips, and A. Franchois, "Weakly convex discontinuity adaptive regularization for 3D quantitative microwave tomography," *Inv. Prob.*, Vol. 30, No. 8, 085005, 2014.
17. Bai, F., A. Franchois, and A. Pižurica, "3D microwave tomography with huber regularization applied to realistic numerical breast phantoms," *Progress In Electromagnetics Research*, Vol. 155, 75–91, 2016.
18. Wang, F. F. and Q. H. Liu, "A hierarchical Bayesian inversion method for electromagnetic imaging of inhomogeneous objects with piecewise homogeneities," *IEEE Trans. Antennas Propag.*, Vol. 69, No. 5, 2903–2912, May 2021.
19. Babaie-Kafaki, S. and R. Ghanbari, "A descent extension of the Polak-Ribière-Polyak conjugate gradient method," *Comput. Math. with Appl.*, Vol. 68, No. 12, 2005–2011, Sep. 2014.
20. Zwamborn, P. and P. M. van den Berg, "The three-dimensional weak form of the conjugate gradient FFT method for solving scattering problems," *IEEE Trans. Microw. Theory Techn.*, Vol. 40, No. 9, 1757–1766, Sep. 1992.
21. Geffrin, J. M., P. Sabouroux, and C. Eyraud, "Free space experimental scattering database continuation: Experimental set-up and measurement precision," *Inv. Prob.*, Vol. 21, No. 6, 117–130, 2005.